

Impact point model predictive control of a spin-stabilized projectile with instability protection

Proc IMechE Part G:
J Aerospace Engineering
0(0) 1–11
© IMechE 2013
Reprints and permissions:
sagepub.co.uk/journalsPermissions.nav
DOI: 10.1177/0954410013514743
uk.sagepub.com/jaero



Matthew Gross¹ and Mark Costello^{1,2}

Abstract

Most smart projectile control systems generate lateral control forces to guide the round to a target. Experience has shown that under the right combination of body orientation, translational velocity, and angular velocity, relatively low lateral control force inputs can induce instability of the round. To solve this problem, an additional control logic layer is appended to a nominal impact point flight control law to protect it from instability in these infrequent, but consequential situations. To highlight the newly developed control logic, a smart 155 mm spin-stabilized projectile equipped with a rotating paddle control mechanism is considered. For this example configuration, cross range maneuvering occasionally induces instability. Simulation results, using both rigid and multi-body nonlinear flight dynamics models, indicate that the addition of the instability protection layer in the control logic prevents projectile instability while not substantially altering target impact statistics. The nature of this protector design lends itself well to the use of a GPU to perform the calculations, greatly decreasing the computation time needed.

Keywords

Projectile, flight dynamics, flight control, impact, point

Date received: 7 August 2013; accepted: 30 October 2013

Introduction

There are a wide variety of physical control mechanisms used to actively control projectiles. The most common of these mechanisms use aerodynamic forces to achieve control. Canards are a very common control mechanism used on all types of projectiles, typically consisting of a pair of canards mounted on the nose of the projectile that, when deflected, produce a normal and axial force on the projectile.^{1,2} Other types of mechanisms can be used to create aerodynamic asymmetries which can be used to guide a projectile. Some examples are spoilers mounted at the rear of a fin-stabilized projectile³ and a spin-stabilized projectile with a nose capable of moving relative to the projectile body.^{4,5} Other types of control mechanisms are pulse jets and thrusters^{6,7} and moving internal parts to achieve trajectory alteration.^{8–11} The main feature of these control mechanisms is the generation of lateral forces and moments employed to guide the projectile to an intended target. Another characteristic feature of these control mechanisms is the relatively low control authority that they possess. For example, it is typical for smart, indirect fire projectiles shot to a range of 25 km to be capable of altering its impact point by a

few hundred meters. The typical low level of control authority associated with smart projectiles has led to the term “ballistic nudging” to describe active control of projectiles.

There are a multitude of control algorithms for use as part of a smart projectile system. Of the various choices for control logic, model predictive control (MPC) is a popular method which is very effective for projectile applications. MPC works by using a dynamic model of the system and determining the control needed to track a desired trajectory with minimal control effort by projecting the state of the system forward in time.^{12–15} MPC logic specialized to direct impact point control stands out as efficiently utilizing available control authority as all control action is focused on moving the impact point to the desired target. An example of this approach is

¹Guggenheim School of Aerospace Engineering, Georgia Institute of Technology, Atlanta, GA, USA

²Woodruff School of Mechanical Engineering, Georgia Institute of Technology, Atlanta, GA, USA

Corresponding author:

Mark Costello, Guggenheim School of Aerospace Engineering, Georgia Institute of Technology, 270 Ferst Drive, Atlanta, GA 30332, USA.
Email: mark.costello@ae.gatech.edu

described by Burchett and Costello¹⁵ where they created an impact point MPC law for a direct fire rocket using a ring of lateral pulse jets. A modified version of projectile linear theory was created to propagate the trajectory to the target plane at an arbitrary point in the trajectory.

While lateral loads are used to effectively steer projectiles, it is well known that these same loads can induce instability under the right set of circumstances. In these situations, the angle between the projectile axis of symmetry and the aerodynamic velocity vector grows beyond tolerable limits and the round tumbles as it falls to the ground.^{16,17} This type of instability leads to very large impact point errors where the projectile falls far short of the target due to high drag. Short rounds not only miss an intended target, but they also endanger friendly forces in the local operation area. The well-known phenomenon of spin-yaw resonance is partially driven by lateral forces excited on the projectile from mass and aerodynamic asymmetries.^{18–23}

The contribution of this paper is additional control logic to an impact point MPC strategy to prevent instability induced by lateral control forces and moments. The paper begins with a description of the mathematical model used to make predictions and is followed by a description of an impact point model predictive controller. This is followed by a detailed description of the projectile instability protector. The proposed methodology is explored in simulation with an example 155 mm spin-stabilized projectile equipped with a paddle control mechanism. Results indicated the proposed method is an effective means to prevent control-induced instabilities.

Smart projectile system dynamics model

Simulation results shown in this paper use a standard six degree of freedom dynamics model with gravity, aerodynamic, and control forces and moments. The orientation of the projectile body is given by the aerodynamic standard 3-2-1 Euler angle sequence as seen in Figure 1. The motion of the projectile center of mass is given by equations (1) to (4).²⁴

$$\begin{Bmatrix} \dot{x} \\ \dot{y} \\ \dot{z} \end{Bmatrix} = \begin{bmatrix} c_\theta c_\psi & s_\phi s_\theta s_\psi - c_\phi s_\psi & c_\phi s_\theta c_\psi + s_\phi s_\psi \\ c_\theta s_\psi & s_\phi s_\theta s_\psi + c_\theta c_\psi & c_\phi s_\theta s_\psi - s_\phi c_\psi \\ -s_\theta & s_\phi c_\theta & c_\phi c_\theta \end{bmatrix} \begin{Bmatrix} u \\ v \\ w \end{Bmatrix} \quad (1)$$

$$\begin{Bmatrix} \dot{\phi} \\ \dot{\theta} \\ \dot{\psi} \end{Bmatrix} = \begin{bmatrix} 1 & s_\phi t_\theta & c_\phi t_\theta \\ 0 & c_\phi & -s_\phi \\ 0 & s_\phi/c_\theta & c_\phi/c_\theta \end{bmatrix} \begin{Bmatrix} p \\ q \\ r \end{Bmatrix} \quad (2)$$

$$\begin{Bmatrix} \dot{u} \\ \dot{v} \\ \dot{w} \end{Bmatrix} = \frac{1}{m} \begin{Bmatrix} X \\ Y \\ Z \end{Bmatrix} - \begin{bmatrix} 0 & -r & q \\ r & 0 & -p \\ -q & p & 0 \end{bmatrix} \begin{Bmatrix} u \\ v \\ w \end{Bmatrix} \quad (3)$$

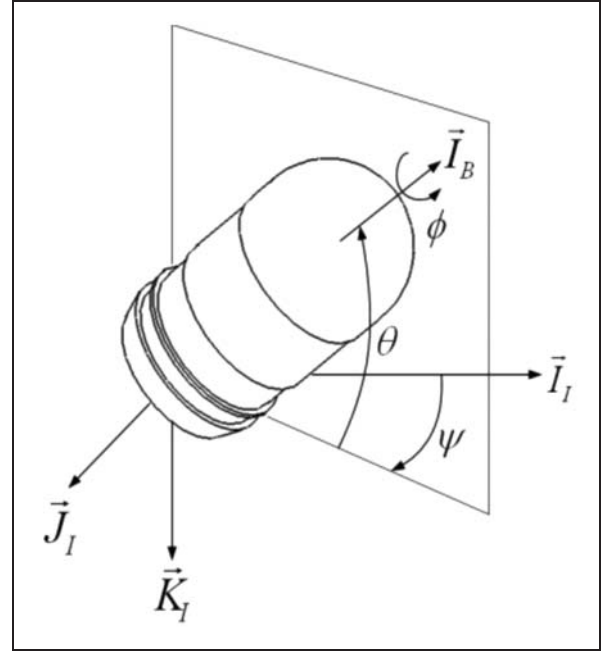


Figure 1. Projectile orientation definition.

$$\begin{Bmatrix} \dot{p} \\ \dot{q} \\ \dot{r} \end{Bmatrix} = [I]^{-1} \left(\begin{Bmatrix} L \\ M \\ N \end{Bmatrix} - \begin{bmatrix} 0 & -r & q \\ r & 0 & -p \\ -q & p & 0 \end{bmatrix} [I] \begin{Bmatrix} p \\ q \\ r \end{Bmatrix} \right) \quad (4)$$

In equations (1) and (2), the shorthand notation $s_\alpha = \sin(\alpha)$, $c_\alpha = \cos(\alpha)$, and $t_\alpha = \tan(\alpha)$ is used. The forces and moments depicted in equations (3) and (4) are total forces and moments acting on the projectile which include aerodynamic (A), gravity (G), and control forces (C). The total forces and moments are given in equations (5) and (6).

$$\begin{Bmatrix} X \\ Y \\ Z \end{Bmatrix} = \begin{Bmatrix} X_A \\ Y_A \\ Z_A \end{Bmatrix} + \begin{Bmatrix} X_G \\ Y_G \\ Z_G \end{Bmatrix} + \begin{Bmatrix} X_C \\ Y_C \\ Z_C \end{Bmatrix} \quad (5)$$

$$\begin{Bmatrix} L \\ M \\ N \end{Bmatrix} = \begin{Bmatrix} L_A \\ M_A \\ N_A \end{Bmatrix} + \begin{Bmatrix} L_C \\ M_C \\ N_C \end{Bmatrix} \quad (6)$$

The aerodynamic forces on the projectile are modeled using existing ballistic expansions with known coefficients given in equation (7).

$$\begin{Bmatrix} X_A \\ Y_A \\ Z_A \end{Bmatrix} = Qd \begin{Bmatrix} -C_{X_0} + C_{X_2} \frac{v^2 + w^2}{V} \\ -C_{N_\alpha} \frac{v}{V} + C_{Y_{pa}} \frac{w \, pd}{V \, 2V} \\ -C_{N_\alpha} \frac{W}{V} + C_{Y_{pa}} \frac{v \, pd}{V \, 2V} \end{Bmatrix} \quad (7)$$

In this equation, Q is the dynamic pressure, d is the aerodynamic reference area, C_{X_0} is the zero-yaw axial force coefficient, C_{X_2} is the yaw-squared axial force coefficient, C_{N_α} is the normal force derivative coefficient, $C_{Y_{pa}}$ is the Magnus force coefficient, and $V = \sqrt{u^2 + v^2 + w^2}$ is the total velocity of the projectile. The weight of the projectile expressed in the projectile body reference frame is given by:

$$\begin{Bmatrix} X_G \\ Y_G \\ Z_G \end{Bmatrix} = \begin{Bmatrix} -s_\theta \\ s_\phi c_\theta \\ c_\phi c_\theta \end{Bmatrix} mg \quad (8)$$

The aerodynamic moments acting on the projectile are the pitching, pitch damping, Magnus, and roll damping moments. Pitching and Magnus moments are given by taking the cross product of the normal and Magnus forces given in equation (7) with the position vector from the center of mass to the center of pressure and location of Magnus force, respectively. The total aerodynamic moments are given in equation (9).

$$\begin{Bmatrix} L_A \\ M_A \\ N_A \end{Bmatrix} = S_B(\vec{r}_{P \rightarrow CP}) Q d \begin{Bmatrix} -C_{X_0} + C_{X_2} \frac{v^2 + w^2}{V} \\ -C_{N_\alpha} \frac{v}{V} \\ -C_{N_\alpha} \frac{w}{V} \end{Bmatrix} + S_B(\vec{r}_{P \rightarrow CM}) Q d \begin{Bmatrix} 0 \\ C_{Y_{pa}} \frac{w}{V} \frac{pd}{2V} \\ C_{Y_{pa}} \frac{v}{V} \frac{pd}{2V} \end{Bmatrix} + Q d^2 \begin{Bmatrix} C_{l_p} \frac{pd}{2V} \\ C_{m_q} \frac{qd}{2V} \\ C_{m_q} \frac{rd}{2V} \end{Bmatrix} \quad (9)$$

Here, $S_B(\vec{r}_{P \rightarrow CP})$ is the skew-symmetric operator acting on the position vector from the center of mass to the center of pressure expressed in the projectile body frame. Similarly, $S_B(\vec{r}_{P \rightarrow CM})$ is the skew-symmetric operator acting on the position vector from the center of mass to the center of pressure of the Magnus force. C_{l_p} is the roll damping coefficient and C_{m_q} is the pitch damping coefficient. Given a control system to generate the control forces X_C, Y_C, Z_C and control moments L_C, M_C, N_C , equations (1) to (4) can be numerically integrated forward in time to generate a trajectory for a smart projectile configuration.

Impact point MPC with instability protection

Nominal control law

Impact point control is a very powerful and useful methodology for smart projectile control that has its roots in MPC.^{12–15} This type of control is especially

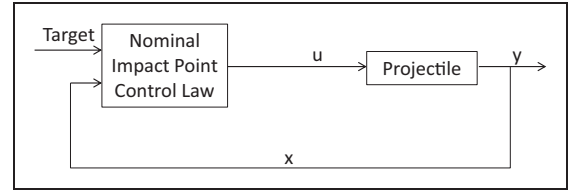


Figure 2. Control system diagram.

applicable to smart projectiles where control authority is small and control is achieved by effectively “nudging” the projectile towards the target. This control law is based on computing multiple trajectories in flight to determine the impact location of a projectile given a varying control input. Using this data, a mapping is determined from the control input to impact locations. This mapping is then used to determine the required control input to impact a specified target. The general form of this control law is shown as a block diagram in Figure 2. The control law receives the target location and the state, and outputs a control input which is used by the actuator to control the projectile.

In order to provide context for the control logic, consider a control mechanism that is capable of generating a lateral load on the projectile in a specific direction in the $\bar{J}_B - \bar{K}_B$ plane. The single control input is the angle of the lateral load in this plane. Suppose this angle is given by ϕ_C . Thus, the control logic must select the lateral control force angle, ϕ_C , at each cycle of control law computation. The locus of all possible control angles yields a control footprint. This footprint can be characterized using an ellipse fit on the impact points. The equation of the ellipse is parameterized by the following equations

$$x_I = A \sin(\phi_C - \phi_0) + x_B \quad (10)$$

$$y_I = B \cos(\phi_C - \phi_0) + y_B \quad (11)$$

In these equations, the command angle ϕ_C and the controlled impact points (x_I, y_I) are known. The ballistic impact point (x_B, y_B) , offset angle ϕ_0 , and constants A and B are the ellipse fit parameters that are estimated from the data or solved using a linear least squares regression of the data. With the ellipse fit, a diagram such as Figure 3 can be drawn to illustrate the control problem. In this illustration, the vector \vec{n}_ϕ spans the entire border of the ellipse and the vector \vec{n}_T is the vector from the estimated ballistic impact point to the target. The command angle required to move towards the target is the angle that aligns these two vectors so that they are parallel. This is equivalent to setting the cross product of the two vectors to zero. Simple algebraic manipulation

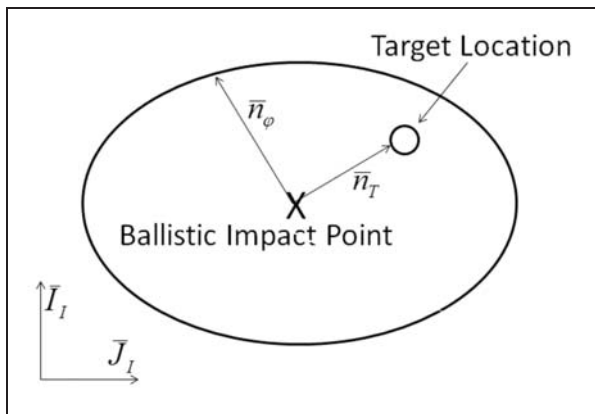


Figure 3. Illustration of impact control model.

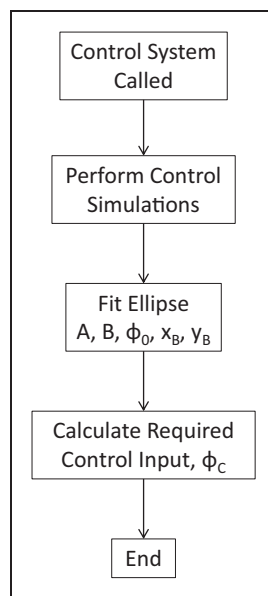


Figure 4. Impact point control law flow chart.

yields equation (12) which is used to calculate the required ϕ_C .

$$\phi_C = \tan^{-1} \left(\frac{B(x_T - x_B)}{A(y_T - y_B)} \right) + \phi_0 \quad (12)$$

Here, (x_T, y_T) is the target location. The command angle is calculated every time the control system is called. The general flow of the control law is shown in Figure 4. The update rate on the control system is based on what is computationally possible. If it takes 1.5 s to perform a simulation and four simulations are needed to estimate the ellipse, then the control system can only update every 6 s. In this sense, it is necessary to use a minimum number of impact points in order to fit the ellipse and minimize computation time in flight. This update time decreases as the flight continues because less of the trajectory needs to be simulated as the projectile gets closer to the ground.

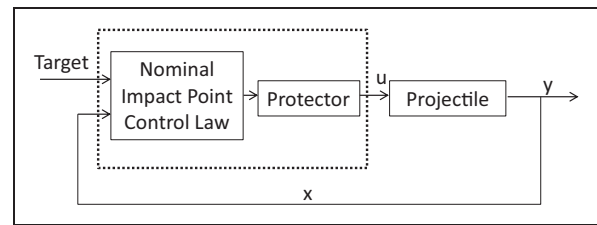


Figure 5. Control system protector diagram.

Instability protector design

The control system protector is an additional layer of control logic that is added to the existing control law that is called in the event of a detected instability and computes a stable control input. Figure 5 is a modification of Figure 2 with the nominal controller and the protector together forming the protected control system. Here, the protector is placed between the nominal controller and the projectile such that when it is called, it will give the projectile a new control input in order to maintain stability. To implement the protector for the impact point controller, the above control law is modified. When the control system is called the first time, four evenly distributed command angles are used to fit the ellipse. For all subsequent control calls, the four command angles used are selected in the neighborhood of the previous command angle. This is done to limit the possibility that one of the control simulations is unstable. To fit the ellipse, a fifth simulation is performed which only has the drag component of the paddle. This impact point is used as the ballistic impact point for the ellipse fit. A sixth simulation is conducted with the calculated command angle to verify that this input is stable. If one of these trajectories is unstable, the protector routine is invoked. This process is shown in the flowchart given in Figure 6. Here, M is a counter for each simulation and N is the total number of simulations run for the nominal impact control law.

The protector routine is in the same spirit as this general control law. A certain number of simulations are performed, simulating the projectile from the current state to the ground, each with evenly spaced command angles between 0° and 360° . This is distinct from the nominal control law in that there are a larger number command angles used which span the entire unit circle as opposed to just a neighborhood of angles. These simulations are separated into stable and unstable groups. Figure 7 shows an example case of the stable and unstable command angles plotted on the unit circle. As can be seen, there is a clear region of stable command angles. The ellipse fit is then generated based on only the stable impact points, as the unstable impact points are not accurate and are to be avoided. With the ellipse fit, the command angle is calculated using the same method. If the command angle is within the unstable region, the command angle is set to the nearest stable command

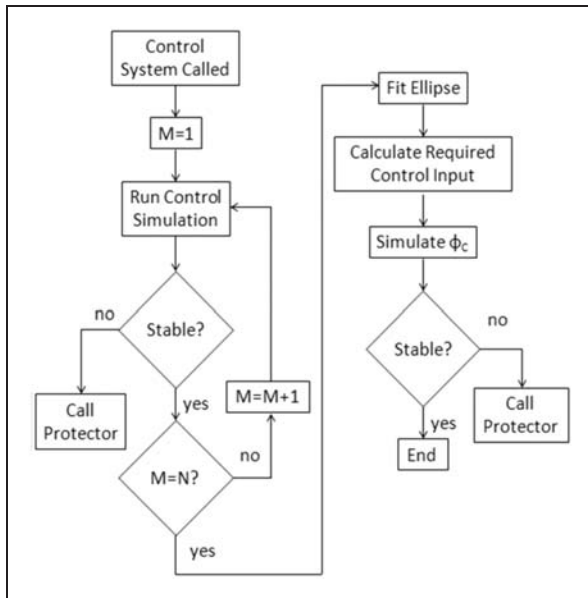


Figure 6. Control system protector flow chart.

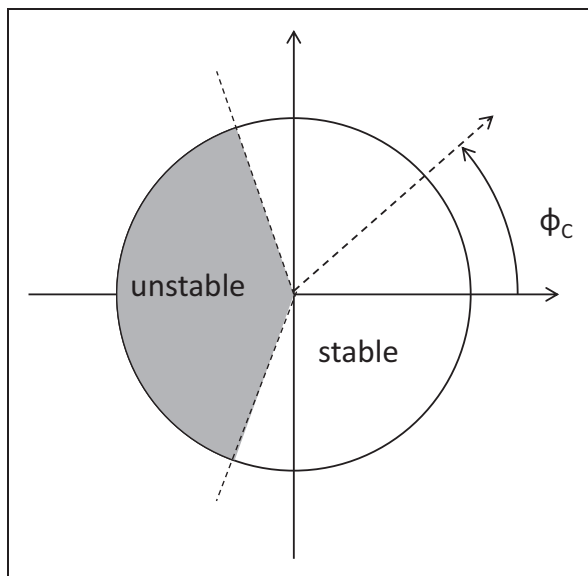


Figure 7. Stable and unstable command angles.

angle, ensuring the projectile remains stable until the next time the control system is called.

Application to an example smart projectile

In order to explore the control logic described above, consider a standard 155-mm, spin-stabilized, artillery round. This projectile is a common large caliber round used for many applications. This projectile is equipped with a control mechanism that uses a paddle as the primary flow effector. The physical properties of the projectile and paddle are given in Table 1. This configuration has a single paddle mounted flush with the rear of the projectile and 0.0695 m from the

Table 1. Physical properties of projectile and control mechanism.

Physical property	Projectile	Paddle
Mass (kg)	46.1725	0.03
Diameter (m)	0.155	0.016
Length (m)	0.843	0.24
Center of gravity - l_p (m)	0.290	0.012
Center of gravity - J_p (m)	0.0	0.0
I_{xx} (kg-m ²)	0.17061	9.6e-7
I_{yy} (kg-m ²)	2.03385	1.92e-6
I_{zz} (kg-m ²)	2.03385	1.92e-6
$I_{xy} = I_{yx}$ (kg-m ²)	0.0	0.0
$I_{xz} = I_{zx}$ (kg-m ²)	0.0	0.0
$I_{yz} = I_{zy}$ (kg-m ²)	0.0	0.0

centerline of the projectile. This paddle is able to rotate relative to the projectile body such that it is externally exposed for a portion of the roll cycle. Figure 8 shows a drawing of the deployed paddle with a closeup view of the control mechanism. Here, a rotary motor which is coupled through a flywheel and clutch to a wedge-shaped paddle extends beyond the surface of the spin-stabilized projectile to create an aerodynamic asymmetry. The motor spins opposite the projectile with an approximately equal magnitude in spin rate. The motor can spin independently when the clutch is disengaged or directly drive the paddle when the flywheel face and clutch are mated. The resulting motion of the paddle when the clutch is engaged is to rotate in and out of the artillery shell in sync with the spin of the projectile, but in the opposite direction. When the paddle is activated to deploy at a particular roll angle window during each revolution, a consistent aerodynamic force and moment is generated that causes a predictable and repeatable deflection in the trajectory in a prescribed roll orientation.²⁵ This control mechanism has shown to have a large control authority due to the rear location and its control force magnitude. Cross range corrections of up to 1 km can be achieved. The nature of the applied force and moment of this mechanism is similar to an impulse where the magnitude cannot be controlled and the paddle force is only active for a portion of the roll cycle.^{1,26}

The forces acting on the paddle can be modeled as an axial force coefficient C_{XC} and normal force coefficient C_{NC} . The paddle also produces a yawing moment given by the cross product of the control forces given in equation (13) with the position vector from the projectile center of mass to the center of pressure of the paddle. These coefficients are all functions of Mach number and were determined using computational fluid dynamic simulations of the paddle attached to the projectile.²⁷ Since the paddle is only exposed for a portion of the roll cycle, the forces are not applied constantly. To

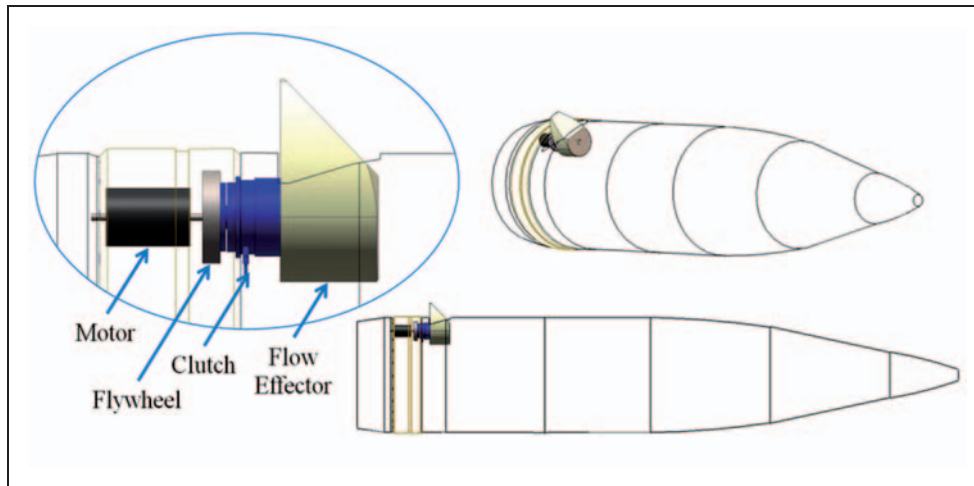


Figure 8. Concept for guided spin-stabilized projectile.

simplify the model used for control calculations, the forces and moments are averaged over the entire roll cycle. The parameter τ is used to represent the scaling of the control force due to this time averaging. Therefore, the simplified model treats the paddle as a constant force acting in direction ϕ_C which is the commanded angle of the paddle. The forces and moment due to the paddle are given in equations (13) and (14).

$$\begin{Bmatrix} X_C \\ Y_C \\ Z_C \end{Bmatrix} = -\tau Q d \begin{bmatrix} 1 & 0 & 0 \\ 0 & c_\phi & s_\phi \\ 0 & -s_\phi & c_\phi \end{bmatrix} \begin{bmatrix} 1 & 0 & 0 \\ 0 & c_{\phi_C} & -s_{\phi_C} \\ 0 & s_{\phi_C} & c_{\phi_C} \end{bmatrix} \times \begin{Bmatrix} C_{XC} \\ C_{NC} \\ 0 \end{Bmatrix} \quad (13)$$

$$\begin{Bmatrix} L_C \\ M_C \\ N_C \end{Bmatrix} = S(\vec{r}_{P \rightarrow CP_C}) \begin{Bmatrix} X_C \\ Y_C \\ Z_C \end{Bmatrix} \quad (14)$$

The launch conditions are as follows: initial velocity of 821 m/s, roll rate of 1650 rad/s, and pitch angle of 45° . The projectile was commanded to a ground target of $(x,y) = (22500,900)$ m which is a ballistic correction of approximately 124 m given an uncontrolled impact point of $(22451,786)$ m. The value of τ is set to 0.3. The control timing is based on each simulation initially requiring 1.2 s to run. The update rate is decreased by 5% each time the control system is called. Figures 9 to 14 show the time histories of the states of the projectile, both uncontrolled and controlled. The controlled impact point is $(22300, 900.5242)$ m, yielding a miss distance of 0.63 m. For the uncontrolled case, 78.85 s elapsed before impacting the ground while for the controlled case 79.8 s elapsed. The ballistic shot reaches a maximum angle of attack of about 1.95° while the controlled shot reaches a maximum of about 2.5° .

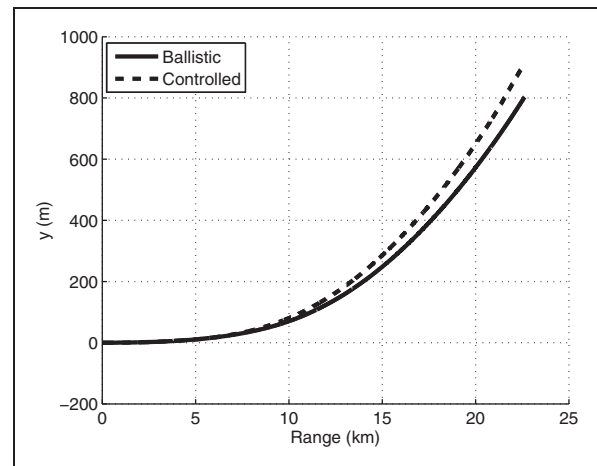


Figure 9. Inertial-Y position vs. range, stable controlled.

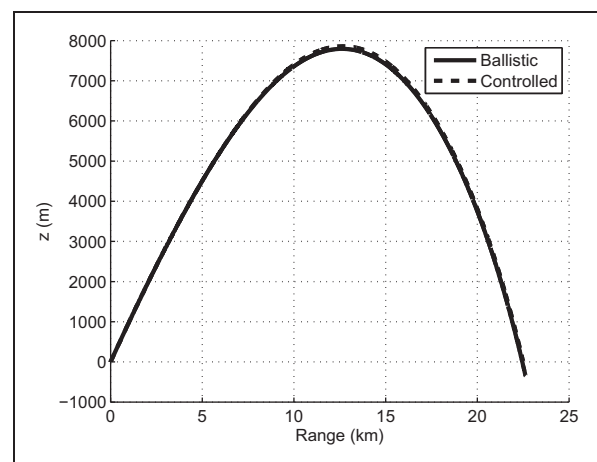


Figure 10. Inertial-Z position vs. range, stable controlled.

To test the protector design, a case is considered using the same initial conditions as the previous simulation with a target of $(22300,1000)$ m and a τ value of 0.3. Forty-eight command angles are used in the

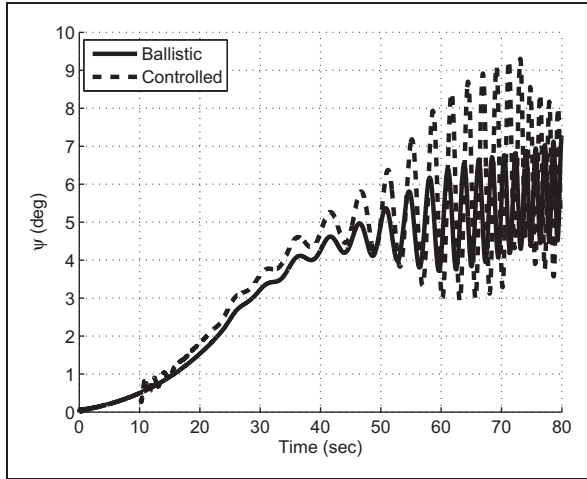


Figure 11. Yaw angle vs. time, stable controlled.

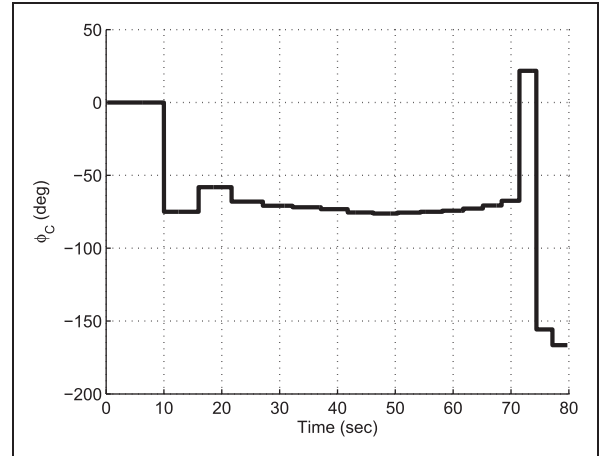


Figure 14. Paddle command angle vs. time, stable controlled.

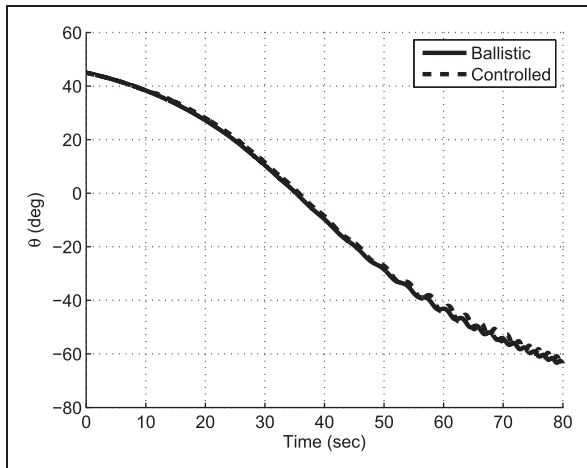


Figure 12. Pitch angle vs. time, stable controlled.

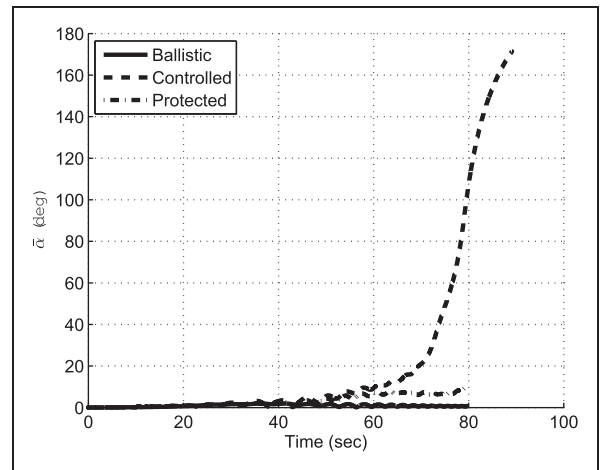


Figure 15. Total angle of attack vs. time, controlled with protector.

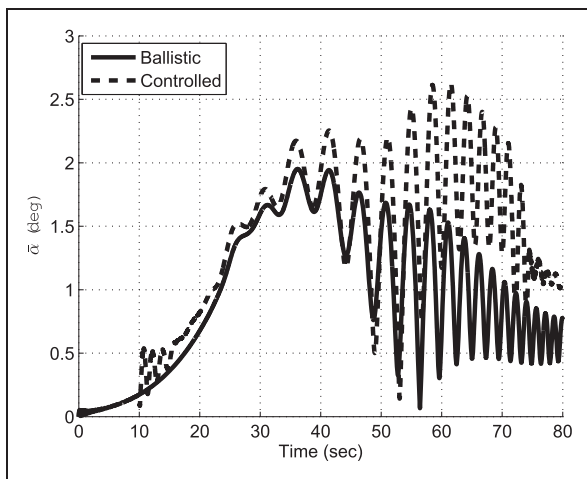


Figure 13. Total angle of attack vs. time, stable controlled.

protector routine. Figure 15 shows the angle of attack profile for the ballistic, controlled, and protected cases. Towards the end of the flight, the angle of attack of the controlled case grows very rapidly,

indicating that the projectile has gone unstable. However, with the addition of the protector, the projectile remains stable throughout the entire flight. The protected projectile had an impact point of (22300, 1000.1) m yielding a miss distance of 0.1235 m. The trajectories of the controlled and protected simulations are very similar until the nominal controlled shot begins to go unstable. Figure 16 shows the command angle of the controlled and protected cases. The protector is first called at about 27 s, giving a different command angle than the nominal controller suggests. While the projectile is stable at this time, the calculated nominal command angle would force the projectile into an unstable region later in the flight. The protector controller corrects for this problem with a different command angle in order to maintain stability. The protector is called again at 32 and 46 s. The protector successfully keeps the projectile stable allowing the control system to continue to run normally for the remainder of the flight. At around 60 s, the large fluctuations in command angle are due to the projectile being aligned with the target and the

command angle changes as it attempts to remain aligned with the target. For this case, the protector is only called a few times, with the majority of control calls not activating the protector.

Figures 17 to 19 show the impact points of Monte Carlo simulations for the uncontrolled, nominal controlled, and protected controlled cases with the circular error probable (CEP) drawn with a solid line. The initial condition standard deviations used for this analysis are given in Table 2. These initial conditions were chosen to represent the range of disturbances such a projectile experiences at launch. The target used was (22325, 779.88) m which is the impact point of the nominal initial conditions with only the drag of

the paddle. For this simulation, the ballistic CEP was 173.2 m and the controlled CEP was about 2 m with 66.5% hitting the target which is defined as landing within 5 m of the target. However, 7.1% went unstable. The majority of the unstable shots lie in a region which would require a command angle close to 0° or 180°. This is in line with previous research by Lloyd and Brown¹⁶ which showed that forces applied laterally to a projectile and parallel with the ground caused instabilities to arise during flight. Note that the CEP cannot be seen in Figures 18 and 19 because it is so small. With the addition of the protector, all 1000 simulated shots remained stable. The number that hit within 5 m of the target increased to 71.5% and the CEP was reduced to 1.6715 m. In this case, the

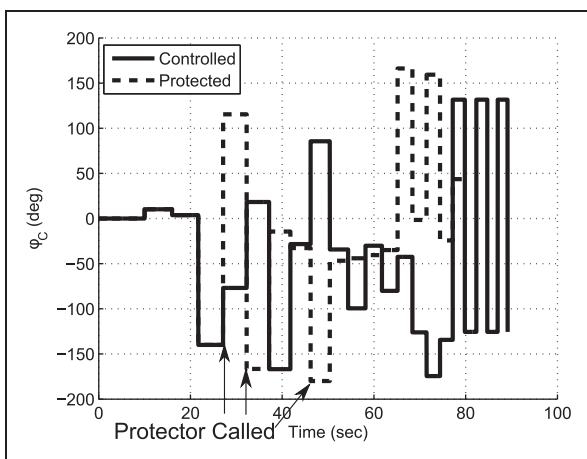


Figure 16. Paddle command angle vs. time, controlled with protector.

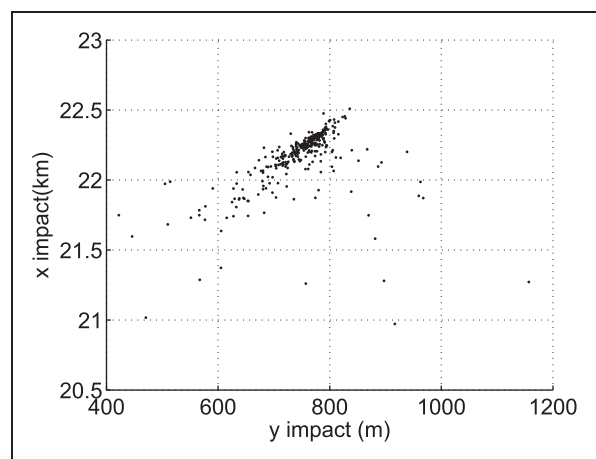


Figure 18. Monte Carlo results, controlled. CEP = 2 m.

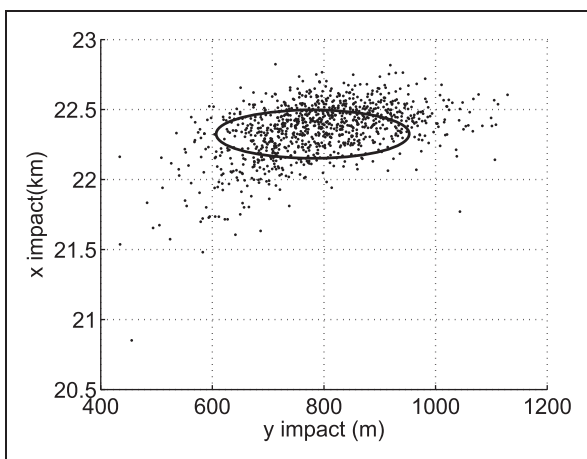


Figure 17. Monte Carlo results, uncontrolled. CEP = 173.2 m.

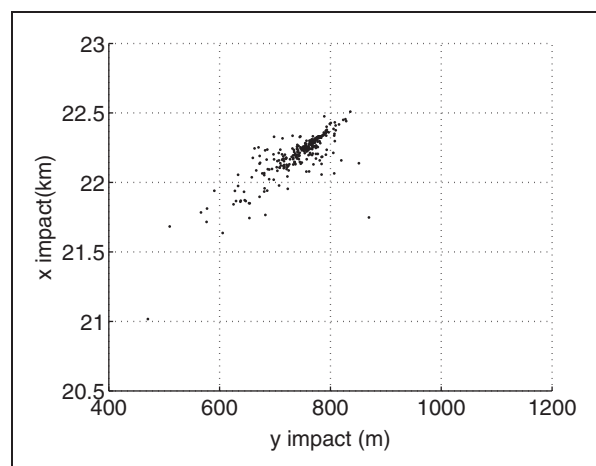


Figure 19. Monte Carlo results, protected. CEP = 1.67 m.

Table 2. Standard deviations of initial conditions used in Monte Carlo simulation.

x(m)	y(m)	z(m)	θ (rad)	ψ (rad)	u(m/s)	v(m/s)	w(m/s)	p(rad/s)	q(rad/s)	r(rad/s)
1	1	1	0.5	0.0002	3.5	2	2	10	2	2

protector was able to completely remove the instability while increasing the performance of the overall control system. This can be seen by the tightening of the impact points as well as fewer impact points far away from the target. The ones that do remain far away from the target are points where the uncontrolled trajectories were also far away from the target.

It is also interesting to view the performance of the protector over different τ values. In this way, τ is used as a scaling factor to observe the control authority of the paddle mechanism. The values tested varied from 0.1 to 0.5 with all other conditions held constant. In each case, the target location was the drag only impact point for each τ value. For the low τ values, the nominal controller remained stable for all cases, therefore, the protector was never needed. As τ is increased, the number of unstable shots increases, requiring the protector to be called more often. Figure 20 shows the CEPs of the controlled and protected cases for each τ value. At small τ , the control authority is not sufficient to overcome the perturbations to the initial state and steer a large number of rounds to the target. The controlled CEP reaches a minimum at a τ of 0.2 and then is effectively constant, increasing slightly with increasing τ . The protector reduces the CEP slightly by steering some of the unstable shots close to the target. The number of stable shots is seen in Figure 21. Without the protector, an increasing number of shots go unstable as τ is increased, while every simulated shot remains stable when the protector is added. Finally, Figure 22 shows the number of shots which hit within 5 m of the target for each τ value. Initially, the number of hits increases with τ before peaking at $\tau=0.3$. The drop-off in hit percentage is due to the increase in unstable shots, which, if stable, may have hit the target. The protector is able to increase the number of shots hitting the target, but also peaks at $\tau=0.35$. While every shot is stable with the protector, the more times the protector is called,

the further off course the projectile is steered in order to maintain stability, preventing the controller from steering it back to the target once stability is achieved.

This protector design shows great performance for smaller τ values, however, when tested with much larger values, the performance decreases significantly. While the protector is able to keep the projectile stable in all cases, the accuracy is greatly diminished. This is because as the paddle effectiveness is increased, the number of unstable command angles increases as well, reducing the number of potential stable command angles. When the protector is called, it must choose a command angle that steers the projectile too far away from the target and is unable to correct for this deviation. In addition, the projectile is more likely to go unstable, which means the protector is called more frequently, greatly increasing computation time. This protector is designed to correct for the occasional or rare instability and is not able to fix highly unstable controlled smart projectiles.

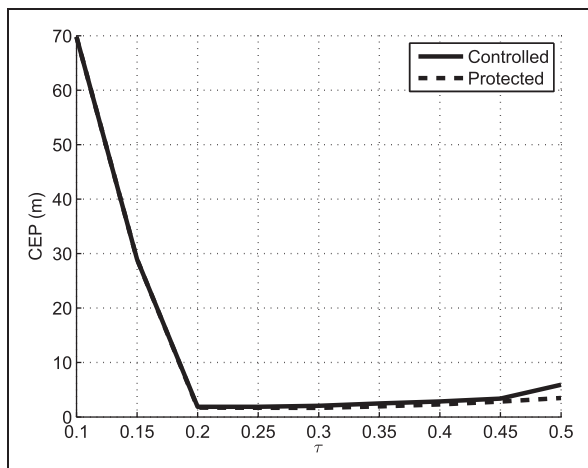


Figure 20. Monte Carlo CEP vs. τ .

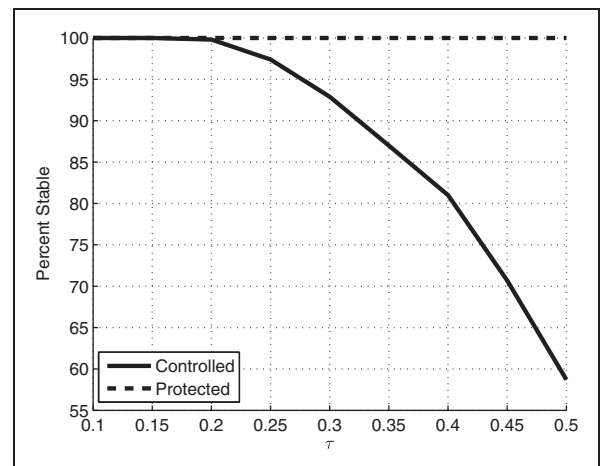


Figure 21. Monte Carlo percent stable vs. τ .

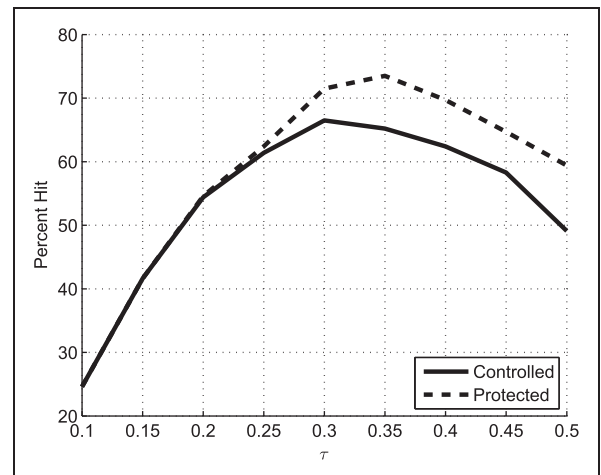


Figure 22. Monte Carlo percent hit vs. τ .

The design of protector is more computationally intensive than the standard control system due to the need to run a large number of simulations each time the protector routine is called. The nature of this design lends itself very well to being parallelized, specifically with applications to using a GPU to perform shot simulations. With the use of a GPU running in parallel, it would be possible to run significantly more simulations at each protector call without significant increase in computation time. These additional simulations could be used to obtain a more accurate characterization of the stable and unstable control regions or to perform Monte Carlo simulations in flight to account for potential errors or disturbances in each simulation. While this protector design was tailored specifically for this control mechanism and control law, the principle can be applied to any control mechanism that uses a single input from the control system.

Conclusion

Many modern smart projectile control mechanisms utilize lateral forces as a means of guiding a projectile towards a target. However, under the right circumstances, these forces are capable of driving a projectile unstable during flight, causing the round to tumble and fall far short of the target, potentially causing collateral damage or friendly fire. In the case of the example smart projectile system considered in detail here (spin-stabilized 155-mm projectile with a paddle control mechanism), instabilities occurred, albeit infrequently, and under very specific conditions. These instabilities were caused by the control system applying certain paddle command angles which would lead the projectile to go unstable later in the flight. The stability protection control logic proposed here successfully prevented projectiles from instability while still maintaining excellent impact point statistics. While results shown above were for a specific smart projectile system, the stability protection control logic can be applied to other smart projectiles, different nominal control laws, and different physical control mechanisms.

Funding

This research received no specific grant from any funding agency in the public, commercial, or not-for-profit sectors.

Conflict of interest

None declared.

References

1. Fresconi F and Plostins P. Control mechanism strategies for spin-stabilized projectiles. *J Aerosp Eng* 2010; 224: 979–991.
2. Fresconi FE. Experimental flight characterization of asymmetric and maneuvering projectiles from elevated gun firings. *J Spacecraft Rockets* 2012; 49: 1120–1130.
3. Patel M, Sowle Z, Ng T, et al. Range and end-game performance assessment of a smart projectile using hingeless flight control. *AIAA paper 2006-671* 2006.
4. Costello M and Peterson A. Linear theory of a dual-spin projectile in atmospheric flight. *J Guid Control Dyn* 2000; 23: 789797.
5. Landers MG, Hall LH, Auman LM, et al. Deflectable nose and canard controls for a fin-stabilized projectile at supersonic and hypersonic speeds. In: *AIAA applied aerodynamics conference*, Orlando, FL, 2003.
6. Davis B, Malejko G, Dorhn R, et al. Addressing the challenges of a thruster-based precision guided mortar munition with the use of embedded telemetry instrumentation. *ITEA J* 2009; 30: 117–125.
7. McMichael J, Lovas A, Plostins P, et al. Microadaptive flow control applied to a spinning projectile. *AIAA paper 2004-2512* 2004.
8. Rogers J and Costello M. Control authority of a projectile equipped with a controllable internal translating mass. *J Guid Control Dyn* 2008; 31: 1323–1333.
9. Frost G and Costello M. Linear theory of a rotating internal part projectile configuration in atmospheric flight. *J Guid Control Dyn* 2004; 27: 898–906.
10. Frost G and Costello M. Control authority of a projectile equipped with an internal unbalanced part. *J Dyn Syst Meas Control* 2006; 128: 1005–1012.
11. D'Amico W. Comparison of theory and experiment for moments induced by loose internal parts. *J Guid Control Dyn* 1987; 10: 14–19.
12. Ollerenshaw D and Costello M. Model predictive control of a direct fire projectile equipped with canards. *J Dyn Syst Meas Control* 2008; 130: 061010, 1–11.
13. Fresconi F and Ilg M. Model predictive control of agile projectiles. In: *AIAA atmospheric flight mechanics conference*, Minneapolis, MN, 2012.
14. Slegers N. Model predictive control of a low speed munition. In: *AIAA atmospheric flight mechanics conference and exhibit*, Hilton Head, SC, 2007.
15. Burchett B and Costello M. Model predictive lateral pulse jet control of an atmospheric rocket. *J Guid Control Dyn* 2002; 25: 860–867.
16. Lloyd KH and Brown DP. Instability of spinning projectiles during terminal guidance. *J Guid Control* 1979; 2: 65–70.
17. Murphy CH. Instability of controlled projectiles in ascending or descending flight. *J Guid Control* 1981; 4: 66–69.
18. Ananthkrishnan N, Raisinghani SC and Pradeep S. Transient resonance of rolling finned projectiles. In: *Proc IMechE, Part G: J Aerospace Engineering* 1999; 213: 97–103.
19. Price DA Jr. Sources, mechanisms, and control of roll resonance phenomena for sounding rockets. *J Spacecraft* 1967; 4: 1516–1525.
20. Murphy CH. Some special cases of spin-yaw lock-in. *J Guid* 1989; 12: 771–776.
21. Murphy CH and Mermagen WH. Spin-yaw lock-in of a rotationally symmetric missile. *J Guid Control Dyn* 2009; 32: 377–382.
22. Murphy CH. Symmetric missile dynamic instabilities. *J Guid Control* 1981; 4: 464–471.
23. Nicolaidis JD. *Two non-linear problems in the flight dynamics of modern ballistic missiles*. Report no. 59-

- 17, January 1959. New York, NY: Institute of Aeronautical Sciences.
24. Etkin B. *Dynamics of atmospheric flight*. Mineola, NY: Dover Publications, 2000.
25. Fresconi F, Cooper GR, Celmins I, et al. Flight mechanics of a novel guided spin-stabilized projectile concept. *J Aerosp Eng* 2012; 226: 327–340.
26. Ollerenshaw D and Costello M. Simplified projectile swerve solution for general control inputs. *J Guid Control Dyn* 2008; 31: 1259–1265.
27. Whyte R, Hathaway W and Friedman E. *Analysis of free flight transonic range data of the 155mm, M483A1, and XM795 projectiles*. ARLCD-CR-79016, August 1979. Maryland, MD: U.S. Army Research Laboratory, Aberdeen Proving Ground.

Appendix

Notation

A, B	impact ellipse axes fit parameters	L_C, M_C, N_C	control moment measure numbers in body frame
C_{I_p}	roll damping coefficient	m	mass of projectile
$C_{m_q} + C_{m_{\dot{\alpha}}}$	pitch damping coefficient	p, q, r	components of rotational velocity of projectile body with respect to an inertial observer written in the projectile frame
C_{mC}	pitching moment coefficient of paddle	Q	dynamic pressure of projectile
$C_{m_{\dot{\alpha}}}$	pitching moment derivative coefficient	$\vec{r}_{P \rightarrow CM}$	position vector from the center of mass to the center of Magnus force
$C_{N_{\dot{\alpha}}}$	normal force derivative coefficient	$\vec{r}_{P \rightarrow CP}$	position vector from the center of mass to the center of pressure
C_{NC}	normal force coefficient of paddle	$\vec{r}_{P \rightarrow CP_C}$	position vector from the center of mass to the center of pressure of paddle
C_{X_0}	zero-yaw axial force coefficient	$S_B()$	skew-symmetric operator acting on a given vector expressed in the body frame
C_{X_2}	yaw-squared axial force coefficient	u, v, w	velocity vector scalar numbers in body reference frame
C_{XC}	axial force coefficient of paddle	V	total velocity of projectile
$C_{Y_{pa}}$	Magnus force coefficient	x, y, z	position vector measure numbers in inertial reference frame
d	reference diameter of projectile	X, Y, Z	force measure numbers in body frame
g	gravitational constant	X_C, Y_C, Z_C	control force measure numbers in body frame
I	mass moment of inertia matrix	x_B, y_B	ballistic impact point coordinates
$\bar{I}_B, \bar{J}_B, \bar{K}_B$	projectile body frame unit vectors	x_T, y_T	target impact point coordinates
L, M, N	moment measure numbers in body frame	$\bar{\alpha}$	total angle of attack
		τ	paddle scaling parameter
		ϕ, θ, ψ	Euler roll, pitch, and yaw of the body
		ϕ_0	impact ellipse angle offset parameter
		ϕ_C	paddle activation Euler roll angle